applied sciences

MDPI

Article

Analysis and Optimization of Dynamic and Static Characteristics of Machining Center Direct-Drive Turntable

Bo Huang *, Jian Wang, Bangyu Tan, Jianguo Zhao, Kang Liu and Junxiong Wang

School of Mechanical Engineering, Sichuan University of Science and Engineering, Zigong 643000, China
* Correspondence: huangbojx@suse.edu.cn

Abstract: There are few studies on optimizing the dynamic and static characteristics of direct-drive turntables. In terms of dynamic and static characteristic analysis, most studies only analyze the dynamic and static characteristics of direct-drive turntables in a single machining position and working condition. The optimization is mainly for individual parts without considering the overall structure of the turntable. A multi-objective optimization method based on the back-propagation neural network (BP) and the non-dominated sorting genetic algorithm is proposed to ensure the machining accuracy of the direct-drive turntable, reduce the total mass, and improve its dynamic and static characteristics. In this paper, the workpiece and direct-drive turntable are studied as a whole. Static and modal analyses determine the maximum deformation locations and vulnerable parts of the turntable. Topology optimization analysis was used to find the redundant mass parts. We determined the optimization objectives and dimensional parameters based on the direct-drive turntable's structural and topology optimization results. Using a central composite experimental design, we obtained test points and fitted them to a response surface model using a BP neural network. A multi-objective genetic algorithm then obtained the optimal solution. After multi-objective optimization, we reduced the mass of the direct-drive turntable by 9.02% and 21.394% compared with the topologically optimized and original models, respectively. The dynamic and static characteristics of the direct-drive turntable increased, and a lightweight design was achieved.

Keywords: direct-drive turntable; dynamic and static characteristics; optimization design; multi-objective optimization

Citation: Huang, B.; Wang, J.; Tan, B.; Zhao, J.; Liu, K.; Wang, J. Analysis and Optimization of Dynamic and Static Characteristics of Machining Center Direct-Drive Turntable. *Appl. Sci.* **2022**, *12*, 9481. https://doi.org/10.3390/app12199481

Academic Editors: Hui Liu, Kai Long and Qi Xia

Received: 30 August 2022
Accepted: 16 September 2022
Published: 21 September 2022

1. Introduction

The rapid development of science and technology, computer technology, and advanced manufacturing technology has put forward higher requirements and brought challenges and opportunities for CNC machine tools [1–3]. As one of the core components of the machine tool, the accuracy of stopping, turning, and locking the direct-drive turntable affects the machining accuracy of the components. The direct-drive turntable supports and rotates the workpiece, and its dynamic and static characteristics significantly impact the machining accuracy of the machine [4–6].

The current methods for determining the optimal design of machine tools are comparative optimization of the static characteristics [7], comparative optimization of the dynamic characteristics [8], structural topology optimization, and parametric optimization of the design [9]. Kim et al. [10] studied a small turntable. They used sensitivity analysis for parameters such as tendons, wall thickness, and composite layer thickness for this machine structure model to improve the machine's dynamic characteristics, with good optimization results. SR Besharati et al. [11] used sensitivity analysis for the dimensional parameters that significantly influenced the gantry structure and utilized a multi-objective genetic algorithm and hierarchical analysis to solve for the best candidate sample points in the design sample space to achieve structural optimization of the gantry. R. Neugebauer et al. [12] applied bionic knowledge to optimize the machine column structure. The results

showed that the bionics optimized column mass and intrinsic frequency to a greater extent and with significant results. Shen et al. [13] used an adaptive growth method based on the natural-branching-system growth mechanism to design the structural internal tendon layout. Additionally, the optimization strategy of the overall machine tool was studied using dynamic sensitivity analysis, which significantly improved the machine structure. Liu et al. [14] addressed the thermo-mechanical coupling effect resulting from various load and heat sources during machining. Yi et al. [15] proposed a new method for spindle system design considering the machine tool spindle and material efficiency. The technique was developed by explicitly modeling the energy characteristics of the spindle system, establishing a parametric optimization multi-objective optimization model, and finally, solving the model with an optimization algorithm that can achieve the design of energy-efficient and efficient machine tools. A review of the reliability-based multidisciplinary design optimization theory is presented in the article by Meng et al. [16], mainly including the reliability analysis methods of different uncertainties and the decoupling strategies of reliability-based multidisciplinary design optimization. Further, an optimization problem for a certain operating condition of a turbine runner blade is introduced to illustrate the engineering application of the above method. Liu et al. [17] proposed an optimization method combining rib-form selection and layout as well as dimensional optimization and topology optimization, which they used to optimize the weak components of a model machining center. After optimization, the low-order inherent frequency of the machine tool was improved, which effectively improved the dynamic performance of the machine tool. Jiang et al. [18] used finite element analysis and modal tests to analyze the dynamic characteristics of the whole machine, with the first-order inherent frequency and mass as the optimization objectives. They used a multi-objective genetic algorithm for multi-objective optimization. This method achieved the purpose of rendering the machining center lightweight while simultaneously ensuring the machining center's dynamic and static performance without degradation. Li et al. [19] carried out a multi-level topology optimization design for each weak component for a class of critical structural components of high-speed CNC gantry milling machines. The objective was to reduce the maximum static deformation of the machine tool. The results showed that although the mass of the machine tool increased somewhat, there was a significant reduction in static deformation and inherent frequency, and the optimization effect was pronounced. Yu et al. [20] took a model of a precision horizontal boring and milling center column as the research object. They constructed a response surface model with the fundamental column frequency, maximum static deformation, and mass as the optimization objectives. They used a multi-objective genetic algorithm to find the optimal response surface approximation and obtained the Pareto front solution for multiple optimization objectives. The results showed that the optimized column mass was unchanged, the first-order intrinsic frequency increased, and the maximum static deformation decreased.

From the history of mechanical structure optimization, the optimization effect of a single mode is limited. Mechanical structure optimization is developing from single-mode optimization to multi-mode synergistic optimization and from single-objective to multi-objective optimization. Combining numerous optimization approaches such as size, shape, topology, bionics, and layout, multi-objective optimization is performed on the entire machine tool. At the same time, using new composite materials to achieve a lightweight design is still the trend of machine tool optimization [21].

There are few studies on optimizing the dynamic and static characteristics of direct-drive turntables. In terms of dynamic and static characteristic analysis, most studies only analyze the dynamic and static characteristics of direct-drive turntables in a single machining position and working condition. They do not consider the dynamic and static characteristics of the direct-drive turntable in the position of maximum machining deformation. The effect of optimization is certain, but it is not easy to reach the best; optimization is mainly for individual parts without considering the overall structure of the turntable. In this paper, we treat the workpiece and the direct-drive turntable as a whole as objects.

Under turning and milling conditions, we simulate multiple machining positions of the direct-drive turntable to obtain the corresponding dynamic and static characteristic data and find the weakest machining position. In the weakest position of the direct-drive turntable, we reshape the overall structure and select the optimized dimensional parameters based on the topology optimization of single working conditions and the topology optimization of composite working conditions. Then, multi-objective optimization of the dimensional parameters is carried out to improve the dynamic and static characteristics of the direct-drive turntable and achieve a lightweight direct-drive turntable.

2. Materials and Methods

2.1. Analysis of Direct-Drive Turntable

The direct-drive turntable is one of the critical components of a machining center. Its accuracy will significantly affect the machining accuracy of the workpiece. The object of this paper is the HZD200 direct-drive turntable of the AVC1200/2 vertical machining center of the Changzheng Machine Tool Factory. Its structure is divided into four main parts: a rotating spindle in direct contact with the torque motor rotor, a mounting sleeve in direct contact with the torque motor stator, a YRT bearing that connects the mounting sleeve to the rotating spindle and provides support capability, and a brake system for the direct-drive turntable.

When milling on a machining center, the C-axis of the direct-drive turntable is clamped, and the six degrees of freedom are constrained. A-axis rotation adjusts the workpiece machining position, constrains the other 5 degrees of freedom except for X-direction rotation, and cooperates with the electric spindle to drive the tool for milling the workpiece. During the turning process, the A-axis is fixed with 6 degrees of freedom, and the workpiece and C-axis will change position with the rotation of the C-axis torque motor. Hence, it constrains 5 degrees of freedom, except for the Z-direction rotation, and works with the turning tool to turn the workpiece. The critical parameters of the direct-drive turntable are shown in Table 1. The structure of the direct-drive turntable is shown in Figure 1.

Table 1. Key design parameters of direct-drive turntable.

Type	Parameter	Type	Parameter
Turntable diameter	200 mm	Limit load	65 kg
A-axis rotation range	±100°	Z-direction travel	500 mm
C-axis rotation range	360°	C-axis rotation speed	200 rad/min

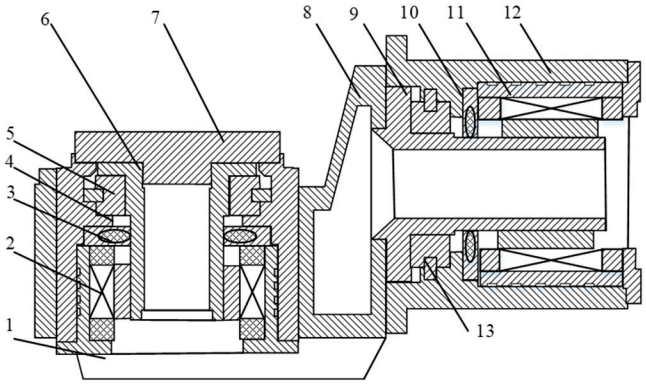

Figure 1. Structure of direct-drive turntable: 1—protective box, 2—C-axis torque motor, 3—pneumatic clamping mechanism, 4—C-axis mounting sleeve, 5—turntable bearing, 6—C-axis rotating spindle, 7—turntable surface, 8—swing frame, 9—A-axis rotating spindle, 10—pneumatic clamping mechanism 2, 11—A-axis torque motor, 12—A-axis mounting sleeve, and 13—turntable bearing 2.

The material of the workpiece studied in this paper is cylindrical gray cast iron. Since the height of the workpiece is unknown, the maximum loading principle is used to calculate

the height of the workpiece. Assuming that the diameter of the turntable surface is the same as the diameter of the workpiece, the maximum mass of the workpiece is 65 kg, as shown in Table 1. The density of HT250 is 7280 kg/m^3, the maximum height of the workpiece is calculated as 280 mm, and the maximum stroke in the Z direction of the AVC1200/2 vertical machining center is 500 mm, so the requirements are satisfied.

2.2. Cutting Force of Direct-Drive Turntable

This paper analyzes the turning and milling conditions. In turning, the direct-drive turntable drives the workpiece to rotate, and the turning cutter makes the feed movement. When milling, the milling cutter rotates rapidly, driven by the motorized spindle as the main motion, and the tool translation motion is the feed motion.

This should provide a concise and precise description of the experimental results, their interpretation, as well as the experimental conclusions that can be drawn.

(1) Calculation of Milling force

The milling force is supposed to be one force, but we decompose the force into the X, Y, and Z directions for easy calculation. The applied position of the milling force and the decomposition of the force are shown in Figure 2.

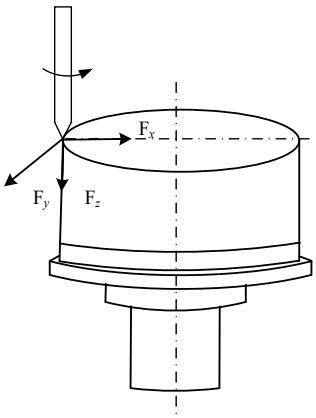

Figure 2. Decomposition of milling force.

The spiral milling cutter is used in milling. The workpiece material is HT250, the power of the motorized spindle is 7.5 kW, the rated speed is 1500 rad/min, the tool diameter d_0 is 50 mm, and the number of teeth Z is 6. The milling adopts symmetric end-milling, The empirical ratios of each milling force during end-milling are listed in Table 2, and the milling force calculation can be expressed by the following Formula (1).

$$F_r = 513\alpha_p^{0.9}\alpha_f^{0.74}\alpha_e^{1.0}Zd_0^{-1.0}K_{Fz} \quad (1)$$

In the formula, α_p is the milling depth, α_f is the feed per tooth, α_e is the milling width, Z is the number of cutter teeth, d_0 is the milling diameter, and K_{Fz} is the correction coefficient.

Table 2. The empirical ratios of each milling force in end-milling.

Cutting Condition	Ratio	Symmetric Milling	Asymmetric Milling	
			Up-Cut-Milling	Climb-Milling
End-milling	F_v/F_z	0.85~0.95	0.45~0.70	0.90~1.00
α_e = (0.4~0.8)d_0	F_e/F_z	0.30~0.40	0.60~0.90	0.15~0.30
α_f = (0.1~0.2) mm/z	F_c/F_z	0.50~0.55	0.50~0.55	0.50~0.55

The milling width is $\alpha_e = 0.6d_0 = 30$ mm; the milling depth α_P is 2 mm, and the amount of feed per tooth $\alpha_f = 0.15$ mm/z. By substituting the parameters into Formula (1),

F_r = 846.55 N. The milling force in each direction is: F_x = 0.9, F_r = 761.895 N, F_y = 0.35, F_r = 296.29 N, F_z = −0.52, and F_r = −440.20 N.

(2) Calculation of Turning Force

The turning force is divided into three forces: the main cutting force F_z, the feeding force F_y, and the back force F_x. According to the data determined in the cutting experiment, the main angle of deflection of the cutting tool is $K_r = 45°$, the tool cutting-edge inclination is $\lambda_s = 0°$, and the rake angle is $\gamma_0 = 10°$. The three calculation formulas of turning force are, respectively:

$$\begin{cases} F_x = 9.81 C_{Fx} \cdot \alpha_p{}^{x_{Fx}} \cdot f^{y_{Fx}} \cdot v_c{}^{n_{Fx}} \cdot K_{Fx} \\ F_y = 9.81 C_{Fy} \cdot \alpha_p{}^{x_{Fy}} \cdot f^{y_{Fy}} \cdot v_c{}^{n_{Fy}} \cdot K_{Fy} \\ F_z = 9.81 C_{Fz} \cdot \alpha_p{}^{x_{Fz}} \cdot f^{y_{Fz}} \cdot v_c{}^{n_{Fz}} \cdot K_{Fz} \end{cases} \quad (2)$$

In the formula, C_{Fx}, C_{Fy}, and C_{Fz} depend on the cutting metals and cutting conditions; x_{Fx}, y_{Fx}, n_{Fx}, x_{Fy}, y_{Fy}, n_{Fy}, x_{Fz}, y_{Fz}, and n_{Fz} are indices of the amount of feed, cutting depth and cutting velocity in the three component forces; K_{Fx}, K_{Fy}, and K_{Fz} are correction coefficients. The coefficients are shown in Table 3:

Table 3. Turning parameters.

C_{Fz}	x_{Fz}	y_{Fz}	n_{Fz}	C_{Fx}	x_{Fx}
92	1.0	0.75	0	54	0.9
y_{Fx}	z_{Fx}	C_{Fy}	x_{Fy}	y_{Fy}	n_{Fy}
0.75	0	46	1.0	0.4	0

Under the tool conditions in this paper, the correction factors K_{Fx}, K_{Fy}, and K_{Fz} are 1.0. the cutting depth during machining is α_p = 3 mm, the amount of feed is α_f = 0.3 mm/z, and the cutting velocity is v_c = 1.4 mm/s. Adding the cutting parameters to Formula (2) gives F_z = 1097.53 N, F_x = 577.18 N, and F_y = 836.36 N.

2.3. Static Characterization

2.3.1. Solid Modeling

We used Solidworks 2020 [22] to build the model of the direct-drive turntable and transferred the 3D model to the Ansys workbench software for analysis. We performed the necessary simplifications in building the solid model. The main methods of simplification are: (1) The geometric model should meet the shared topology, which is conducive to the meshing of the direct-drive turntable model and facilitates the transfer of torque, force, and displacement. (2) We should simplify some features that we can ignore in the model analysis, such as rounded corners, tapered edges, etc. The model is shown in Figure 3.

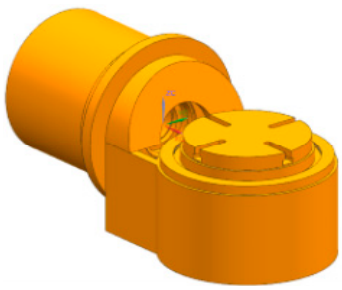

Figure 3. Three-dimensional model of direct-drive turntable.

2.3.2. Adding Materials

The material used in the turntable surface is HT200, the material used in the workpiece is HT250, and the material used in the mounting sleeve and the rotating spindle is 45 steel.

The material used in the swing frame is QT500-7, and the material used in the YRT100 bearing is CCr15. The specific parameters are shown in Table 4.

Table 4. Material parameters of direct-drive turntable.

Material	Density (kg/m^3)	Poisson's Ratio	Elastic Modulus (Pa)
HT200	7.15×10^3	0.23	1.13×10^{11}
45 steel	7.85×10^3	0.3	2.00×10^{11}
QT500-7	7.10×10^3	0.275	1.69×10^{11}
GCr15	7.81×10^3	0.3	2.07×10^{11}
HT250	7.28×10^3	0.27	1.20×10^{11}

2.3.3. Adding Loads and Boundary Conditions

The fixed constraint was added to the bottom of the swing frame and the C-axis in the milling condition. Additionally, the rotation constraints were added to the A-axis. In the turning condition, because a clamping mechanism fixes the A-axis and the swing frame is connected with A-axis and the installation sleeve by bolts, these parts have little effect on the machining accuracy. The C-axis drives the workpiece to rotate and has a great relationship with the static characteristics, so the C-axis was used to analyze the overall static characteristics of the direct-drive turntable turning condition. The fixed rotation was added to the C-axis, and the fixed support was added to the contact part of the mounting sleeve and the swing frame. The decomposition forces in the X, Y, and Z directions were added to different parts of the direct-drive turntable under two working conditions to replace the cutting force. The YRT bearing contact with the rotating spindle supports it and greatly correlates with the turntable's radial positioning accuracy. The YRT bearing adopts elastic support. At the same time, standard earth gravity was applied to simulate gravity.

2.3.4. Element Selection and Grid Division

When selecting the element type, the direct-drive turntable was a tetrahedral element, and the workpiece was a hexahedral element. We selected an element size of 10 mm, generating a total of 342,049 nodes and 174,545 elements of structural strain energy. The finite element model is shown in Figure 4.

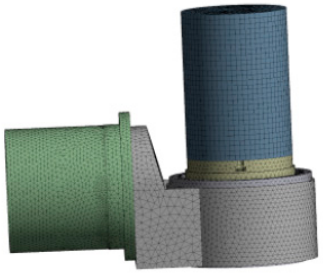

Figure 4. Finite element model of direct-drive turntable.

2.3.5. Selection of Limit Machining Position

The milling cutter machining at different positions affects the direct-drive turntable and workpiece. Therefore, it was is necessary to add milling force at different machining positions of the workpiece for analysis. We set the center of the top part of the direct-drive turntable as the origin. The milling force was added at the edge of the workpiece at a clockwise interval of 10° from the *Y*-axis. We used the same method when turning, as shown in Figure 5:

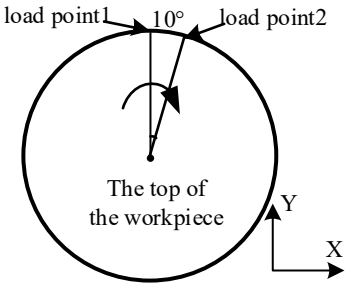

Figure 5. Diagram of cutting force load point position.

2.4. Dynamic Characteristic Analysis

The static characteristics of the direct-drive turntable can only reflect its ability to resist deformation under specific conditions. In the machining process, the direct-drive turntable is not only affected by static load but also has structural deformation under alternate loading. Therefore, the direct-drive turntable not only needs to meet the requirements of static characteristics but must also have good dynamic characteristics.

2.4.1. Modal Analysis

The finite element model of the direct-drive turntable was imported into the Modal module of ANSYS Workbench for modal analysis. Modal analysis does not require additional force such as cutting force and gravity, and the other conditions are the same as the statics. Considering the direct-drive turntable's limited rotational speed and machining conditions, it only reaches a low modal order. Therefore, after the modal analysis, the first six-order modal analysis of the direct-drive turntable was conducted.

The steps of the modal analysis of the direct-drive turntable in the ANSYS Workbench software are as follows: (1) importing the finite element model; (2) determining the material and material performance parameters; (3) meshing setting; (4) setting the boundary conditions; (5) post-processing of modal analysis results; (6) results and analysis.

2.4.2. Direct-Drive Turntable Harmonic Response Analysis

When a direct-drive turntable is used for milling, the tool exerts a force on the workpiece that varies periodically. Under milling conditions, the direct-drive turntable is not susceptible to resonance. Still, the dynamic deformation corresponding to the machining frequency without resonance is superimposed on the static deformation, which may be larger than the maximum deformation allowed if both have the same maximum deformation position. To avoid this situation and to quantify the degree of impact of milling forces on the direct-drive turntable at different machining rates, we should investigate the dynamic response of the direct-drive turntable when subjected to alternating loads to see if it meets the requirements. Therefore, the harmonic response of the direct-drive turntable was analyzed. The machining speed of the direct-drive turntable in the turning condition was much lower than that of the milling condition, so the milling condition was used as a representative for the analysis. The same model as the modal analysis was used for the harmonic response analysis of the direct-drive turntable. The modal analysis data were shared with the Harmonic Response module in the Ansys Workbench software to add milling forces and determine the location and direction of the applied forces, frequency range, and phase angle. In the process of harmonic response analysis, the milling force was taken as a component, and the component forces in the X, Y, and Z directions were taken as 761.895 N, 296.29 N, and 440.20 N, respectively. The sweeping frequency span of the milling force was set to 0–3000 Hz, and the phase angle was set to 0. We wanted to determine whether the inherent frequency of the direct-drive turntable and the dynamic characteristics at the same position were the same after adding loads at different positions. We added milling forces to the direct-drive turntable at the maximum radius and the center

of the machined workpiece. The results were evaluated using amplitude–frequency curves and dynamic stiffness.

2.5. Topology Optimization Analysis

Topology optimization uses mathematical methods to optimize the material distribution, force transmission path, and structural layout of the structure given constraints, loads, and optimization objectives in the design area. In this paper, composite working condition topology optimization and single working condition topology optimization are carried out for the direct-drive turntable. The milling or turning of the direct-drive turntable is often analyzed separately, and topology optimization of a group of working conditions with significant influence is carried out. Although optimizing a set of working conditions can save time, this solution is not necessarily optimal for other conditions or is even entirely unsuitable for other working conditions.The static analysis results of the direct-drive turntable are shared in the topology optimization module of Ansys Workbench. The optimization problem is defined according to the actual needs, the optimization region and response constraints are set, the optimization results are output, and the model is re-established according to the results. Then, the optimized model is analyzed to determine whether it meets the working requirements. If it does not meet the working requirements, topology optimization is carried out again, or other optimization methods are selected.

2.5.1. Variable Density Method

In the variable density method, the density of the finite element of the optimization model is regarded as changing. Additionally, the relative density of the model varies within the interval (0, 1) with the force condition. The penalty function is introduced. By setting the threshold value, Ansys Workbench software will delete densities of the finite element less than the threshold value, while those greater than the threshold value will be retained. The interpolation model used in this paper is Solid Isotropic Material with Penalization (SIMP). In the model, the material of the optimization model is isotropic, and the density and properties of the material are exponential functions. The primary expressions of SIMP are:

$$E(\rho) = \rho p E_0, \rho \in [0.001, 1] \tag{3}$$

$$E(\rho) = E_{\min} + \rho p (E_0 - E_{\min}), \rho \in [0.001, 1] \tag{4}$$

In the formula, ρ is the relative density of elements, p is the penalization parameter, which is the power of the density, E is the elastic modulus after interpolation, E_0 is the solid elastic modulus, and $E_{\min}$ is the elastic modulus at the cavity. $E_{\min}$ is set to $E_0/1000$.

The parameters ρ and p control the relative density of elements; the higher the value of p, the more the intermediate density is penalized, and the more the relative density of elements will approach 0 or 1. If the value of p is too high, the function will be difficult to converge. Therefore, the value of p is generally within the interval (2,6). In Ansys Workbench, the default penalty factor p is 3.

2.5.2. Mathematical Model of Topology Optimization

The mathematical model of topology optimization under a single working condition is as follows:

$$\begin{cases} \min c(\rho) = U^T K U = \sum_{e=1}^{N} (\rho_e)^{\mathrm{p}} {u_c}^T k_0 u_e \\ subject\ to \begin{cases} KU = F \\ \frac{V}{V_0} = \frac{\sum_{e=1}^{N} v_e \rho_e}{V_0} \le \eta \\ 0 \le \rho_{min} \le \rho_e \le \rho_{max} \le 1 \end{cases} \end{cases} \tag{5}$$

In the formula, c is the structural strain energy, F is a vector of external force, U is the displacement matrix, K is the stiffness matrix, ρ_e is the relative density of the element material, u_e is the displacement of element nodes, k_0 is the element stiffness matrix, N is the total number of nodes, v_e is element volume, V_0 is the volume before optimization,

and V is the volume after optimization. η is the percentage of retained volume within the interval (0, 1). ρ_{min} and ρ_{max} are the minimum and maximum relative density of materials. To avoid the singularity of the total stiffness matrix, when the relative density of the material is very small, it is treated as a cavity, and its ρ = 0.001.

The linear weighting method was used to add the corresponding weight coefficient to each working condition according to the importance of each working condition. The topological optimization mathematical model of a single working condition of turning and milling was transformed into the mathematical model of the turning–milling composite working condition. The mathematical model is as follows:

$$\begin{cases} \min c(\rho) = \sum_{i=1}^{m} \omega_i c_i = \left\{ \omega_i^p \left[\frac{c_i(\rho_i) - c_i^{min}}{c_i^{max} - c_i^{min}} \right]^p \right\}^{\frac{1}{p}} \\ \quad subject\ to \begin{cases} \sum_{i=1}^{m} \omega_i = 1 \\ \frac{V}{V_0} \le \eta \\ 0 \le \rho_{min} \le \rho_e \le \rho_{max} \le 1 \end{cases} \end{cases} \tag{6}$$

In the formula, ρ_i is the relative density of the element material under the i-th working condition, ω_i is the weight factor for the i-th working condition, m is the total number of working conditions, c is the structural strain energy, ${c_k}^{max}$ and ${c_k}^{min}$ are the maximum and minimum values of the strain energy of the objective function under the i-th working condition.

2.5.3. Single-Condition Topology Optimization

Firstly, the working conditions of the direct-drive turntable were set to the turning and milling mode. We shared the static analysis data of both working conditions in the topology optimization module. The optimized basic parameter settings were as follows: the maximum number of iteration times was 500, the minimum normalized accuracy was 0.001, the convergence accuracy was 0.1%, and the solver type was sequential convex programming.

The setting of boundary conditions was the same as that in the static analysis. The simplified model of the direct-drive turntable was taken as the optimization region, and the workpiece was set as the exclusion region. The optimization models of turning and milling single working conditions were established, respectively. As shown in Figure 6, red is the exclusion region, and blue is the optimization region.

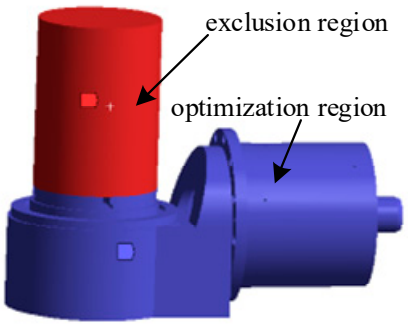

Figure 6. Optimization and exclusion regions of topology optimization.

According to experience, the threshold of 0.3 was more appropriate. Ansys Workbench performed the optimization at 50% and 60% mass retention rates. According to the topology optimization of the removal results of the effect diagram, the results were compared and analyzed. The original model was further reconstructed via structural dimension optimization, and we observed and analyzed the optimization results.

2.5.4. Topology Optimization of Composite Conditions

Topological optimization of the composite conditions needed to be realized via the linear weighting method, and its mathematical model is X = [X1, X2]. In the actual processing, it was considered that the weights of topology optimization of the turning and milling conditions were the same, and the weight factor of X1 was set to 1, and X2 was also set to 1.

2.6. Multi-Objective Optimization

2.6.1. Multi-Objective Optimization Process

With the decrease in mass retention rate, we could see that the A-axis and C-axis of the direct-drive turntable could also be optimized to a certain extent. Therefore, the size optimization method was used to optimize the A-axis and C-axis. As a whole, the direct-drive turntable was optimized using the multi-objective size optimization method. Based on the topology optimization of the direct-drive turntable, the size optimization of the improved direct-drive turntable structure ensured that the dynamic and static characteristics of the direct-drive turntable met the processing conditions to achieve the lightweight design of the direct-drive turntable. The main multi-objective optimization processes were as follows:

(1) In SolidWorks 2020, a parametric design of the size parameters of the direct-drive turntable was carried out. Through the interfaces of ANSYS Workbench and SolidWorks 2020, the three-dimensional model was transformed into a finite element analysis model.
(2) In the topology optimization model, the optimized size parameters were reasonably selected as variables. The constraint range of the optimization parameters was set at 10%, and the constraint condition was to achieve a light weight without reducing the stiffness and the first natural frequency.
(3) Selecting suitable experimental design methods generates finite element analysis samples. The statics and dynamics of each generated sample were analyzed, and the results were analyzed comprehensively.
(4) The response surface between the test site and the optimization objective was established using a BP neural network model.
(5) The non-dominated sorting genetic algorithm (NSGA-II) was used to optimize the response surface many times to obtain the Pareto front solution set. According to the optimization objectives, the most suitable set of optimization data was selected to obtain the optimization results.

2.6.2. Establishment of Response Surface Model

(1) Determination of optimization parameters of direct-drive turntable

We combined the structural characteristics of the direct-drive turntable with the topology optimization results of the composite working conditions and selected the three-dimensional parameters as the optimization parameters on the turntable surface. Three size parameters were chosen on the C-axis, and one size parameter was selected on the A-axis, as shown in Figures 7 and 8. These sizes changed locally without changing the overall size. The selected size optimization range varied within ±10%, and the value ranges are shown in Table 5.

(2) Sensitivity analysis

We investigated the effects of seven design parameters on the turntable's mass, natural frequency, and maximum deformation. Focusing on the parameters with great influence can avoid purposeless structural modification. The theoretical basis of sensitivity can be expressed as follows [23]:

$$S = \frac{df(x)}{dx} \tag{7}$$

In this formula: $f(x)$ is the differentiable function, and S is the sensitivity.

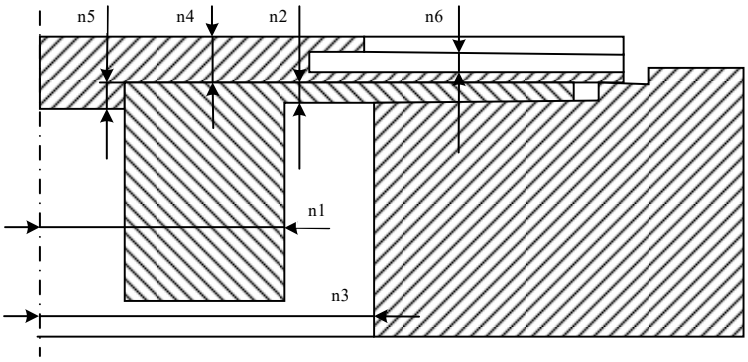

Figure 7. Optimal design parameters of C-axis.

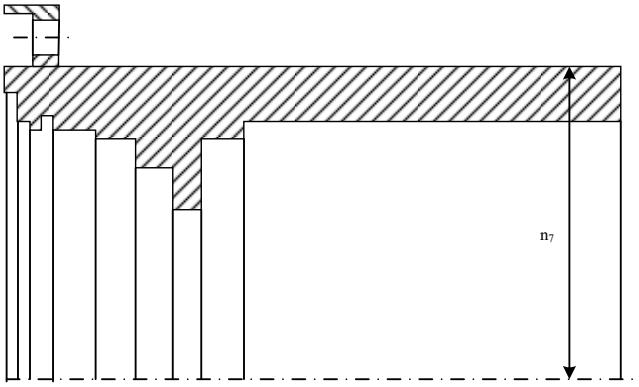

Figure 8. Optimal design parameters of A-axis.

Table 5. Design variables and value ranges.

Optimizing Size Parameters	Initial (mm)	Lower Limit (mm)	Upper Limit (mm)
n_1—C-axis radius	82.14	73.926	90.354
n_2—C-axis support thickness	13.16	11.844	14.476
n_3—Inner diameter of C-axis mounting sleeve	205.78	185.2	226.36
n_4—Thickness of turntable surface	22.81	20.529	25.091
n_5—Thickness of connection between turntable surface and C-axis	10.53	9.477	11.583
n_6—Oil groove depth of turntable	7.27	6.543	7.997
n_7—Outer diameter of A-axis mounting sleeve	235	211.5	258.5

(3) Central composite design

Using a central composite design to determine test points can ensure accuracy and reduce the number of test points [24]. We used the central composite design to design the test points and calculate the values of the corresponding points, and the response surface model was established through these points.

The response surface method is a method that uses an experimental design to obtain the optimal solution for multiple variables. Formula (8) expresses the principle of the response surface method:

$$y(x) = \beta_0 + \sum_{i=1}^{n} \beta_i x_i + \sum_{i=1}^{n} \beta_{ii} {x_i}^2 + \sum_{i=2}^{n} \sum_{j=1}^{i-1} \beta_{ij} x_i x_j \quad (8)$$

In this formula: x represents a set of all the test points, β is an unknown number, and the number of β *is* L = $(n + 1)(n + 2)/2$. When using the least squares method to determine β, the number of test points P must be greater than L.

The relationship between the number of design variables and the number of test points is shown in Table 6.

Table 6. Number of design variables and test points.

Number of Design Variables	1	2	3	4	5	6	7
Factorial coefficient	0	0	0	0	1	1	1
Number of test points	5	9	15	25	27	45	78

Through the optimization and exploration function of the ANSYS Workbench 2020 software, 45 test points were obtained. The first group of data is the original data. The response surface was constructed by fitting the test points. Table 7 shows the central composite design point.

Table 7. Central composite design test point.

Order	n_1 (mm)	n_2 (mm)	n_3 (mm)	n_4 (mm)	n_5 (mm)	n_7 (mm)	f (Hz)	δ_{max} (μm)	m (kg)
1	82.140	13.160	205.780	22.810	10.530	235.000	614.2500	2.8232	110.300
2	82.140	11.844	205.780	22.810	10.530	235.000	616.300	2.8128	110.130
3	82.140	14.476	205.780	22.810	10.530	235.000	611.940	2.8358	110.460
...	...	...	...	...	...	...	...	...	
44	77.392	13.921	217.670	24.128	11.139	221.420	589.330	2.972	100.150
45	86.888	12.399	217.670	24.128	11.139	221.420	605.560	2.868	100.910
46	86.888	13.921	211.6119	24.128	11.139	248.580	601.690	2.888	115.830

(4) Response surface fitting

The BP neural network is one of the most commonly and widely used models. The biggest feature of the BP neural network is that it can establish the high non-linear reflection from the Rn (n is the number of input neurons) space to the Rm (m is the number of output neurons) space by using only some of the sample data [25]. The BP neural network was used to establish the mapping relationship between the test point samples and the optimization objectives, as shown in Figure 9.

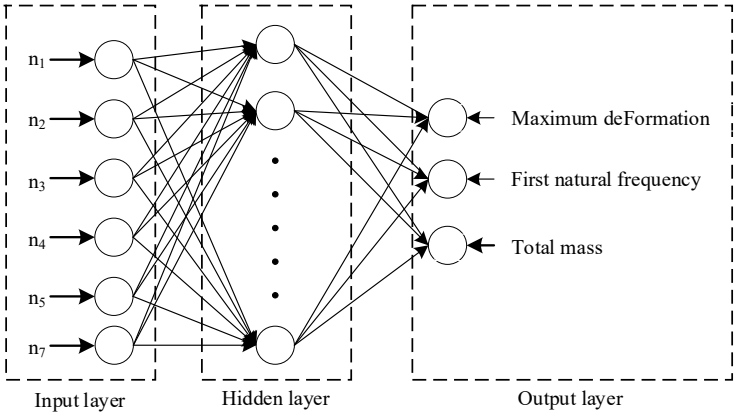

Figure 9. Mapping relationship between sample data and optimization objective.

According to Kolmogorov's theorem [25], the three-layer BP neural network model can approximate any continuous function if only the functional relationship between the input and output layers is linear and the hidden layer is a non-linear increasing function. Therefore, the BP neural network model of Ansys Workbench also has three layers. The input layer comprises six optimized size parameters. The output layer consists of three optimized target parameters: the mass of the direct-drive turntable, the first natural frequency,

and the maximum deformation δ_{max} under milling conditions. Normalization was applied to each datapoint to prevent excessive data variation for each optimization parameter. The learning rate is 0.05, the training error is 10^{-3}, and the maximum number of learning is 2000.

2.6.3. Multi-Objective Optimization Based on Genetic Algorithm

We used the Design Exploration module of ANSYS Workbench to determine the test point via experimental design within the range of multiple design variables. The experimental data were obtained via simulation and calculation. The response surface model of the objective function was constructed by fitting the multiple sets of data, and the appropriate optimization algorithm was selected to process the response surface to obtain the comprehensive optimal target.

A mass change in the direct-drive turntable leads to a change in the turntable structure. It may increase the deformation of the workpiece during the machining process of the turntable and affect the machining accuracy. Therefore, it is necessary to minimize the deformation of the direct-drive turntable. The closing of the machining frequency and the natural frequency may lead to a decline in machining accuracy and even damage the direct-drive turntable. Therefore, the first natural frequency is as large as possible according to the actual situation.

Combined with the parameters obtained from the statics and structural dynamics analysis, the mathematical optimization model is obtained:

$$\begin{cases} \min(y_3(x)) \\ \min(y_4(x)) \\ \max(y_5(x)) \\ X = [x_1, x_2, x_3, x_4, x_5, x_7] \\ X_{iL} < x_i < x_{iU} \end{cases} \tag{9}$$

In this formula: $y_3(x)$ is the total mass of the turntable and workpiece, $y_4(x)$ is the maximum deformation of the turntable and workpiece, $y_5(x)$ is the first natural frequency of the direct-drive turntable, y is the objective function, X is all the design variables, x is a design variable, x_{iL} is the lower limit of the design variable, x_{iU} is the upper limit of the design variables, and x_{iL} and x_{iU} are the constraint conditions.

After multi-objective optimization, a series of optimization solutions that meet the constraint conditions will be generated, and these solutions are called Pareto solutions. To improve the solution precision, finding the solution that meets the requirements as much as possible is necessary. The most suitable optimization result is selected from all the solutions.

John Holland proposes a genetic algorithm under the influence of biological evolution theory. It is an optimization method that uses the concept of animal genetics to solve engineering problems [26]. The optimization exploration module of ANSYS Workbench can carry out multi-objective optimization based on a genetic algorithm. So, a multi-objective genetic algorithm is used to optimize the mathematical model (Formula (9)). The NSGA-II (non-dominated sorting genetic algorithm) is used in this paper and is one of the most effective multi-objective genetic algorithms. According to the non-dominated principle, NSGA-II takes constraints as the processing goal, which can quickly sort non-dominated solutions and maintain high precision and population diversity. If the solution of the genetic algorithm is required to have a global property and not to converge too fast, population uniformity needs to be maintained. The shifted Hammersley sequence sampling method and trade-off function method can meet the above conditions.

The Hammersley sequence sampling technique is a quasi-random number-sampling technique which generates uniformly distributed sample points in the n-dimensional feasible solution region based on the Hammersley algorithm [27]. Hammersley sample points are more concentrated in the starting point area in the K-dimensional hypercube. Shifted Hammersley sampling technology [28] is adopted to make up for this deviation, which moves the sample points based on Hammersley sequence sample points. The sample

points are more evenly distributed. Shifted Hammersley sequence points have a low minimum bias [29]. Here, the Hammersley sample points are offset Δ = N/2 to make them uniformly concentrated in the central area of the design space. To ensure that the multi-objective genetic algorithm converges quickly to the global Pareto optimal solution.

The trade-off function is used to evaluate the mass of the selected sample points. In multi-objective optimization, the constraint and the objective functions are usually quite different in magnitude, so the normalization method is needed to combine the multi-constraint and multi-objective into a single function.

$$Mj = \left(\frac{|y_t - y|}{y_{\max} - y_{\min}} \right)_t \tag{10}$$

In this formula: y_t is the ideal feasible solution of the j-th objective function; y is the current value of the j-th objective function; $y_{\max}$ is the maximum value of the j-th objective function; and $y_{\min}$ is the minimum value of the j-th objective function.

When y is the objective function:

$$y_t = \begin{cases} y, y > y_t^* \\ y_t^*, y < y_t^* \end{cases} \tag{11}$$

If y is a constraint function, when $y > y_t^*$, y_t can be expressed as:

$$y_t = \begin{cases} y, y > y_t^* \\ y_t^*, y \leq y_t^* \end{cases} \tag{12}$$

If y is a constraint function, when $y < y_t^*$, y_t can be expressed as:

$$y_t = \begin{cases} y, y < y_t^* \\ y_t^*, y \geq y_t^* \end{cases} \tag{13}$$

y_t^* is the specified target value. After normalization, the trade-off function is:

$$\phi = \sum_{j-1}^{n} M_j \tag{14}$$

In this formula: n is the sum of the number of objective and constraint functions, and the optimal initial population can be obtained according to Formula (14).

3. Results and Discussion

3.1. Static Characteristic Analysis Results and Discussion

According to the static method of Section 2.3, the deformation rule of the milling condition is solved, as shown in Figure 10:

As shown in Figure 10, when the milling force and Y-axis angle are equal to about 60°, the maximum deformation is 2.9772 μm. This value is the maximum deformation value of the direct-drive turntable milling condition, and its corresponding position is the maximum deformation position. When the milling position is closer to the top of the workpiece, the deformation of the workpiece is larger. Therefore, in the milling process of the direct-drive turntable, the maximum deformation value can be obtained when the angle between the working point of milling force and the Y-axis is 60° and is located on the top surface of the workpiece. The stress nephogram of the maximum deformation position is shown in Figure 11:

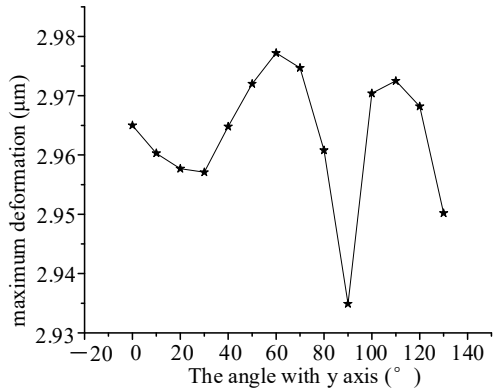

Figure 10. The maximum deformation at different loading positions under milling condition.

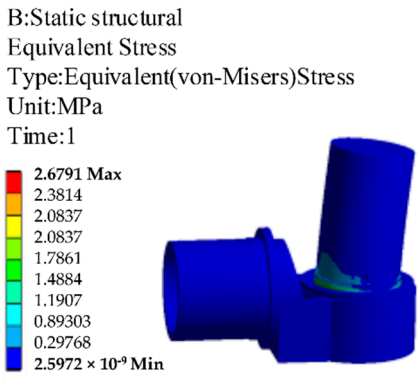

Figure 11. The milling stress nephogram of the maximum deformation position.

Analyzing the stress nephogram of the maximum deformation position, the maximum stress value of the direct-drive turntable under milling force is 2.6791 MPa. The maximum value appears in the milling force addition side of the turntable, and the stress is mainly concentrated at the bottom of the workpiece. The stress of the turntable surface's top and the mounting sleeve's bottom is small. The material of the turntable surface is HT200, and the yield limit is 200 MPa. The maximum stress of the turntable is far less than 200 MPa. The maximum deformation of the direct-drive turntable occurs on the workpiece, and the maximum deformation is 2.9772 μm. According to the processing requirements, the maximum deformation of the workpiece of the direct-drive turntable should be less than 10 μm. The results meet the job requirements.

According to the same research method as that used for the milling condition, the maximum deformation variation law of the turning condition and the stress nephogram and deformation nephogram of the maximum deformation position are obtained, as shown in Figures 12 and 13:

As shown in Figure 12, when the turning force and *Y*-axis angle are equal to about 20°, the maximum deformation is 4.5239 μm. The maximum deformation value of the direct-drive turntable turning condition is 4.5239 μm, and its corresponding position is the maximum deformation position. The stress nephogram at the maximum position of machining deformation is shown in Figure 13. When the direct-drive turntable is turning, the overall stress is small, and the maximum stress is 5.5303 MPa; this is far less than the material yield limit of the turntable surface, whether turning or milling the direct-drive turntable. It is not necessary to worry that the maximum stress will destroy the direct-drive turntable. The direct-drive turntable meets the stiffness and accuracy requirements under the two working conditions.

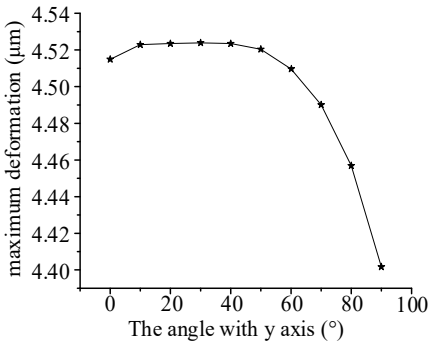

Figure 12. The maximum deformation at different loading positions under turning condition.

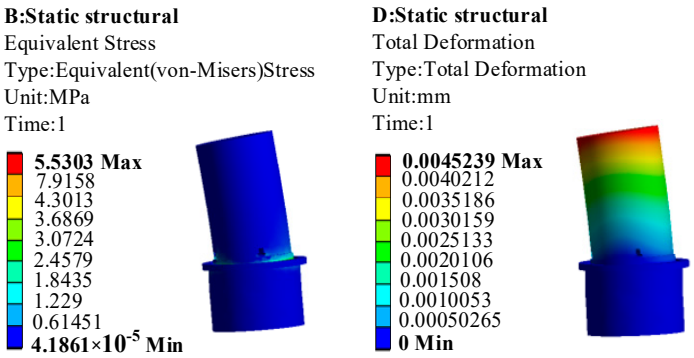

Figure 13. The turning stress nephogram and deformation nephogram of the maximum deformation position.

3.2. Dynamic Characteristic Analysis Results and Discussion

3.2.1. Modal Analysis Results and Discussion under Milling Conditions

The modal analysis of the direct-drive turntable was carried out according to the finite element modal analysis method in Section 2.4.1. The first six modes of the direct-drive turntable under milling conditions are shown in Figure 14.

The first six vibration modes and natural frequencies of the direct-drive turntable under milling conditions are summarized in Table 8.

The first six modes of the direct-drive turntable under turning conditions are shown in Figure 15.

The first six vibration modes and natural frequencies of the direct-drive turntable under turning conditions are summarized in Table 9.

In the first six modes of the direct-drive turntable under the two working conditions, the first four modes are mainly located on the C-axis and the workpiece, and the fourth to sixth modes occur on the overall structure of the direct-drive turntable. Aside from the workpiece, processing should pay more attention to the direct-drive turntable C-axis part.

3.2.2. Dynamic Characteristic Safety Analysis of Direct-Drive Turntable

If the machining frequency is too close to the natural frequency, the workpiece deflection will increase, and resonance will occur. This situation will lead to machining inaccuracy, a direct-drive turntable stiffness decline, and direct-drive turntable internal accessories falling off and causing danger. According to the relationship between rotational speed and frequency:

$$n = 60f \tag{15}$$

In this Formula: f is the frequency (Hz) and n is the rotational speed (rad/min). According to Formula (15), we can convert the direct-drive turntable's first natural frequency into the motorized spindle's machining speed, and the motorized spindle's corresponding

machining speed is 35,659.8 r/min. The spindle speed of the machining center of the direct-drive turntable is 1500 r/min, the milling cutter has six teeth, and the equivalent machining speed is 9000 r/min. Therefore, the direct-drive turntable can avoid resonance in milling. The first natural frequency of the turning condition is 595.06 Hz, and the rotation speed of the torque motor is 200 r/min, so it is more difficult for it to resonate.

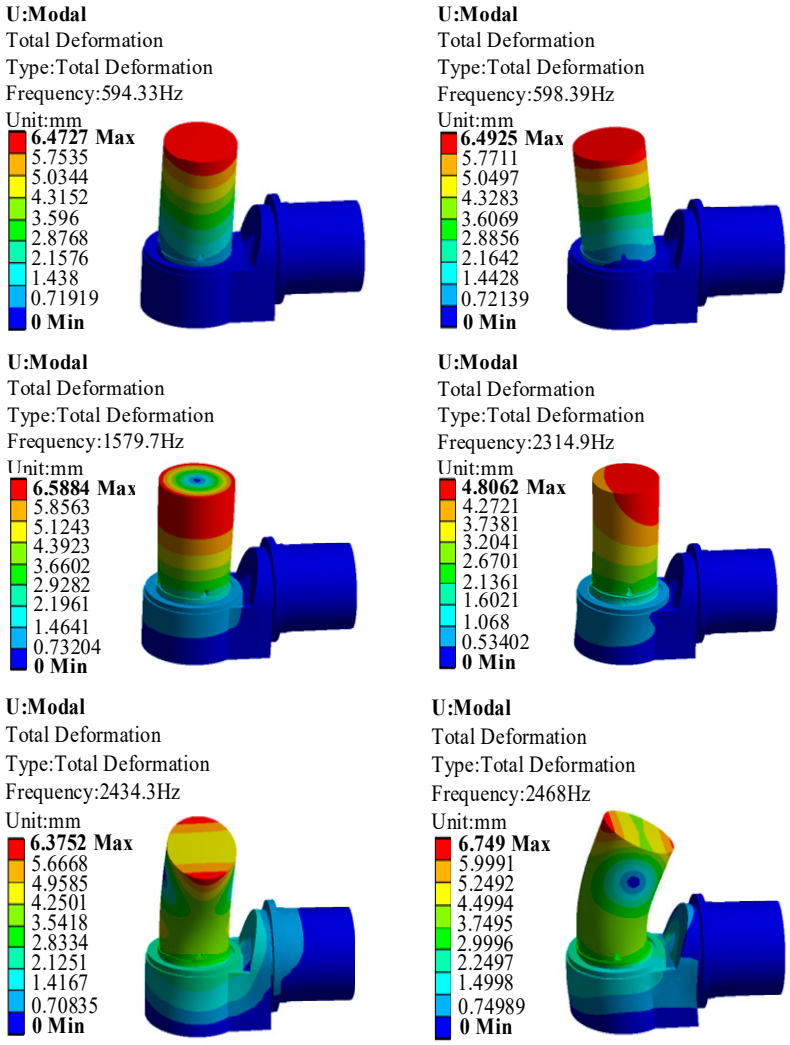

Figure 14. Nephogram of the first six vibration modes under milling conditions.

Table 8. The first six vibration modes and natural frequencies of direct-drive turntable under milling conditions.

Order	Frequency (Hz)	Vibration Mode
1	594.33	C-axis and workpiece oscillating back and forth
2	598.39	C-axis and workpiece oscillating left and right
3	1579.7	C-axis and workpiece rotation
4	2314.9	C-axis and workpiece oscillating up and down
5	2434.3	C-axis, workpiece, and swing frame oscillating back and forth
6	2468	C-axis, workpiece, and swing frame oscillating left and right

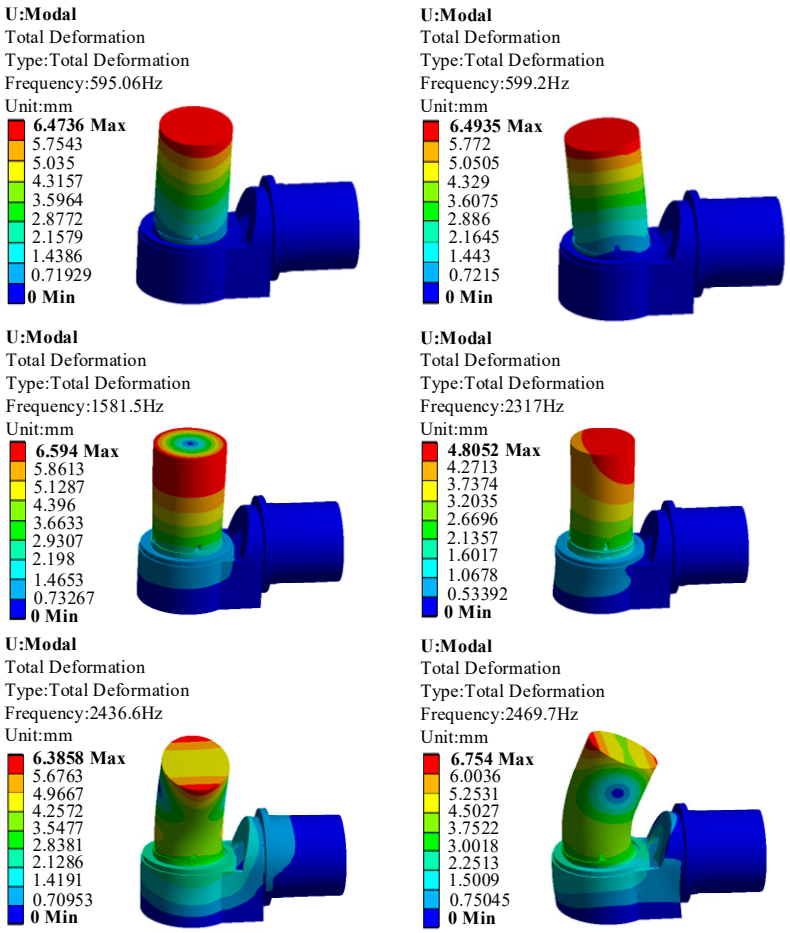

Figure 15. Nephogram of the first six vibration modes under turning conditions.

Table 9. The first six vibration modes and natural frequencies of direct-drive turntable under turning conditions.

Order	Frequency (Hz)	Vibration mode
1	595.06	C-axis and workpiece oscillating back and forth
2	599.20	C-axis and workpiece oscillating left and right
3	1581.5	C-axis and workpiece rotation
4	2317	C-axis and workpiece oscillating up and down
5	2436.6	C-axis, workpiece, and swing frame oscillating back and forth
6	2469.7	C-axis, workpiece, and swing frame oscillating left and right

3.2.3. Harmonic Response Analysis Results and Discussion

(1) Harmonic response analysis of the upper-surface edge of the workpiece

A total of 60 solution schemes were set in the analysis, and 50 Hz was counted once. The amplitude and frequency curves of the direct-drive turntable in the X, Y, and Z directions were analyzed, as shown in Figure 16.

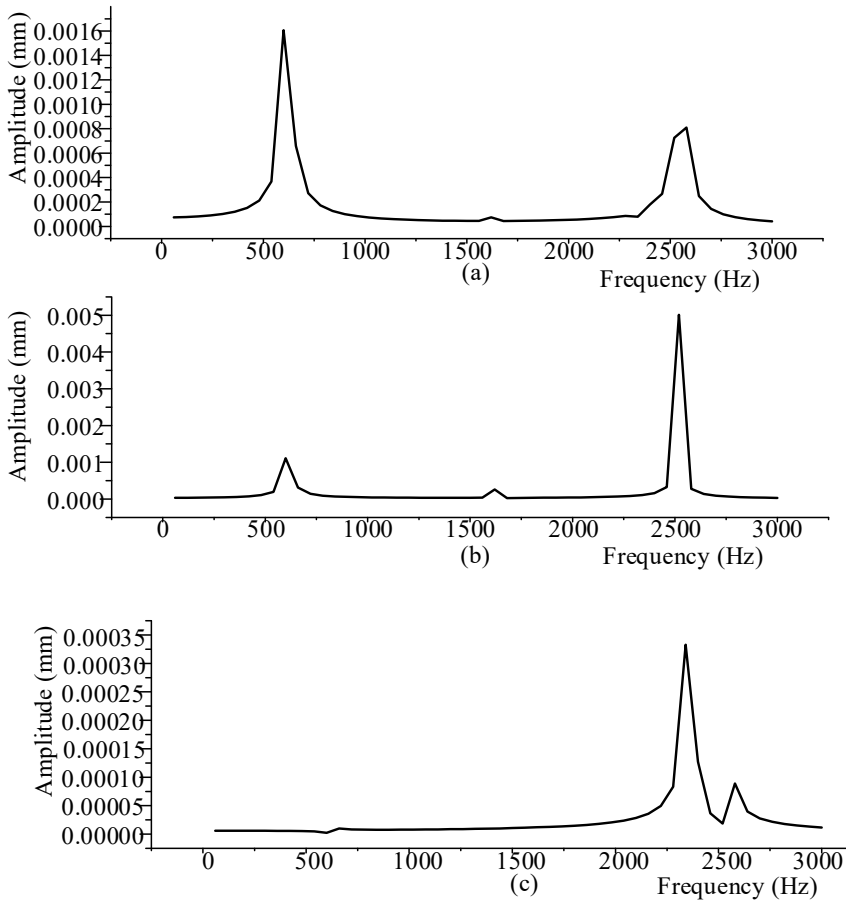

Figure 16. Harmonic response curve of turntable under edge loading: (**a**) X-directional harmonic response curve; (**b**) Y-directional harmonic response curve; (**c**) Z-directional harmonic response curve.

We can find, by comparing the three graphs, that there is a peak in both the X and Y directions when the milling frequency is close to 600 Hz. When the machining frequency increases, the amplitude will return to normal. When the machining frequency of the direct-drive turntable reaches about 1600 Hz and 2300 Hz, the amplitude will rise again. The equivalent speed of the electric spindle driving the tool during milling is about 9000 r/min, i.e., 150 r/s, far from 600 Hz, 1600 Hz, and 2300 Hz. It is observed that the amplitude is small, even when superimposed with static characteristic deformation. It is much less than 10 μm. When the working frequency is near 600 Hz, 1600 Hz, and 2300 Hz, the direct-drive turntable has larger deformation, which corresponds to the first six orders of inherent frequency of modal analysis so that it can prove the correctness of the modal analysis. Therefore, the selected machining frequency for the direct-drive turntable should be far away from these three values to avoid damage to the direct-drive turntable structure.

Since the superposition of the external high-frequency interference and milling force may reach the first-order natural frequency, the point with the natural frequency of 600 Hz was analyzed. Dynamic stiffness is one of the evaluation parameters of the structure's resistance to interference. Each different working speed of the milling force corresponds to a different dynamic stiffness, and the smaller the dynamic stiffness, the worse the structure's resistance to interference. The dynamic stiffness of the direct-drive turntable differs in the three directions, so it needs to be further calibrated by dynamic stiffness. The calculation formula for dynamic stiffness is:

$$K = F/A \tag{16}$$

In the formula, K is the dynamic stiffness, F is the corresponding milling force in each direction, and A is the maximum amplitude in each direction. The maximum deformation

in the X direction is 1.606 × 10^{-3} mm, in the Y direction is 1.109 × 10^{-3} mm, and in the Z direction is 2.295 × 10^{-6} mm; then, the dynamic stiffness in the three directions is Kx = 4.745 × 10^5 N/mm, Ky = 2.678 × 10^5 N/mm, and Kz = 1.918 × 10^8 N/mm. When the milling force is applied to the maximum diameter of the workpiece on the direct-drive turntable, the dynamic stiffness of the turntable surface in the Y direction is the minimum when the frequency of the milling force is around 600 Hz, so when the above constraints are satisfied, the impact on the Y-direction machining accuracy is the greatest.

(2) Harmonic response analysis of the upper-surface center of the workpiece

It is found in Figure 17 that when the milling force is added to the center of the upper surface of the workpiece on the direct-drive turntable, the first peak amplitude of its X, Y, and Z directions also appears at about 600 Hz. The maximum deformation in the X direction is 1.476 × 10^{-3} mm, and the maximum deformation in the Y direction is 8.053 × 10^{-4} mm. The maximum deformation in the Z direction is 9.089 × 10^{-7} mm. The dynamic stiffness is calculated according to the method of calculating Kx = 4.319 × 10^5 N/mm, Ky = 3.688 × 10^5 N/mm, and Kz = 4.843 × 10^{11} N/mm; still, the Y direction has the greatest influence at about 600 Hz under the action of milling force.

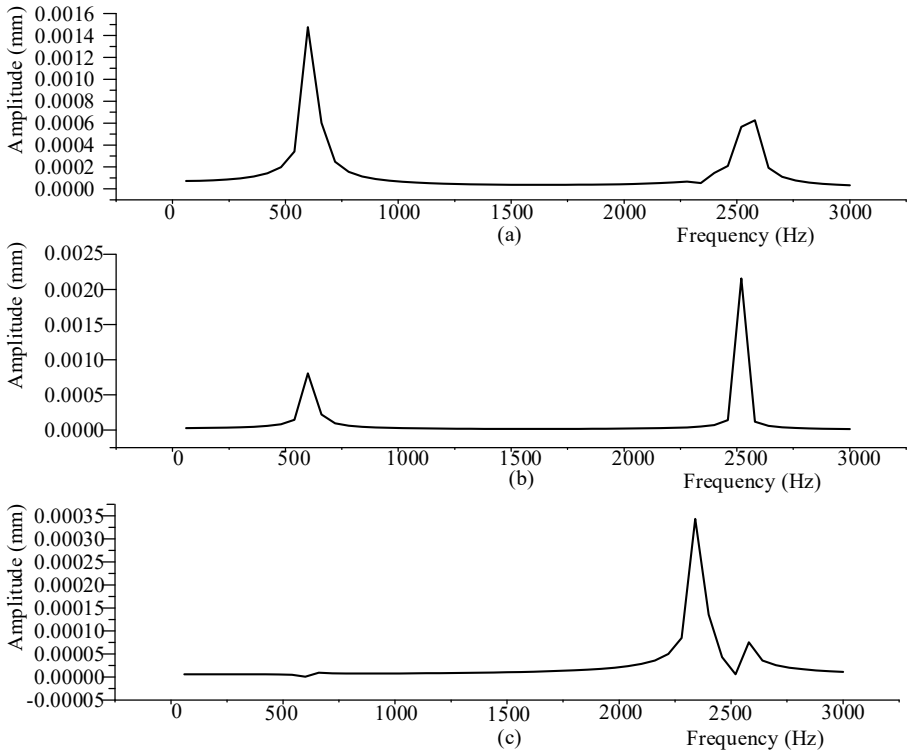

Figure 17. Harmonic response curve of turntable under center loading: (**a**) X-directional harmonic response curve; (**b**) Y-directional harmonic response curve; (**c**) Z-directional harmonic response curve.

A comprehensive analysis of the results of the two different applied load positions in the direct-drive turntable milling condition shows that:

The sum of static and dynamic deformation for the two loading cases reaches a maximum of about 600 Hz. Comparing Figures 16 and 17, We can find that the load addition position has almost no effect on the natural frequency distribution of the direct-drive turntable. Since each peak's frequency does not overlap the excitation frequency provided by the machine tool to the direct-drive turntable, the machine tool can easily avoid the harm caused by resonance to the structure under regular operation.

3.3. Topology Optimization Results and Discussion

To compare the topology optimization analysis of the direct-drive turntable under composite conditions, we imported the statics analysis results of the turning and milling conditions into the topology optimization module to obtain the topology optimization analysis results of the single condition. The mass retention rates are also set to 50% and 60%, and the optimization region is also in the same region. Figure 18 is the topology optimization result of the turning condition, Figure 19 is the topology optimization result of the milling condition, and Figure 20 is the topology optimization result of the composite condition (the red region can be removed, the light red region can be removed or retained, and the grey region is retained).

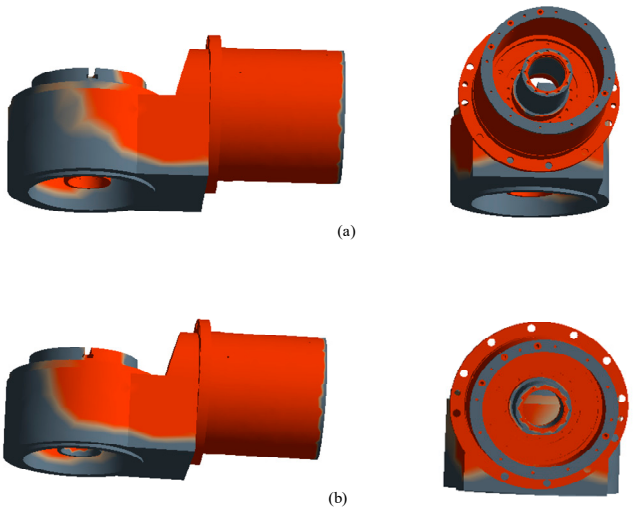

Figure 18. Topology optimization results of direct-drive turntable in turning condition: (**a**) 50% mass retention rate; (**b**) 60% mass retention rate.

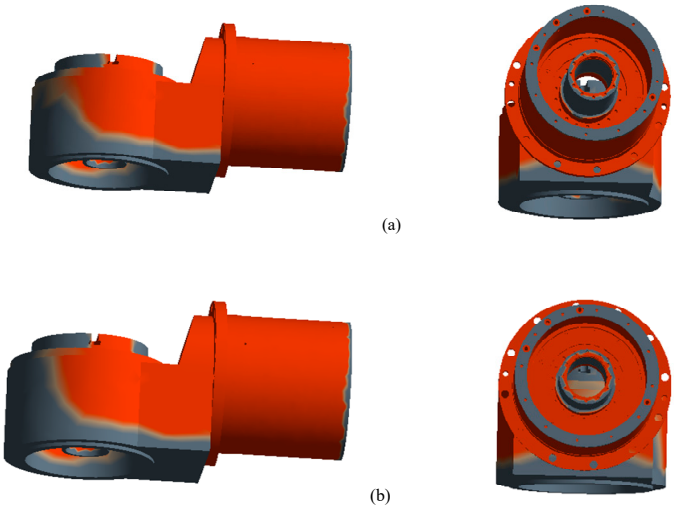

Figure 19. Topology optimization results of direct-drive turntable in milling condition: (**a**) 50% mass retention rate; (**b**) 60% mass retention rate.

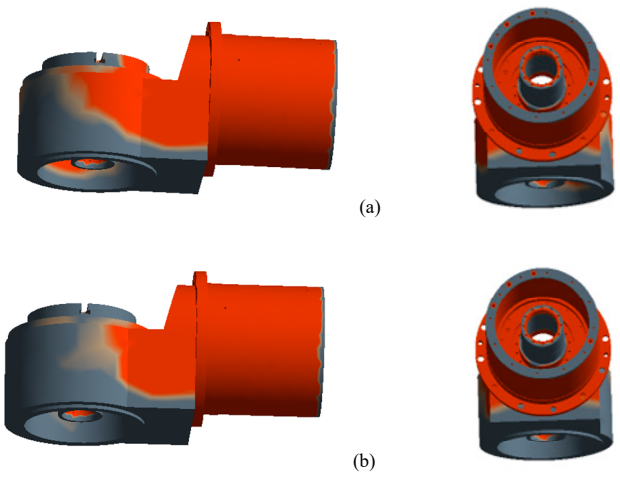

Figure 20. Topology optimization results of direct-drive turntable in composite condition: (**a**) 50% mass retention rate; (**b**) 60% mass retention rate.

By comparing the results of single-condition topology optimization and composite-condition topology optimization, it can be found that the main removed region is the C-axis part of the direct-drive turntable after increasing the percentage of removal mass under the same working condition, and the removed region of other parts has almost no increase. Therefore, the C-axis part of the direct-drive turntable has a certain mass redundancy, and we can adjust its size to a certain extent. By observing the same mass retention rate of the turning and milling topology model, we can find that the two topology models are similar. Still, the topology optimization results are somewhat different due to the constraints and stress conditions. The topology optimization model of the composite working condition of the direct-drive turntable synthesizes the topology optimization results of the two working conditions. It conforms to the stress characteristics of the two working conditions. According to the actual situation and direct-drive turntable topology optimization model, the following conclusions can be drawn by comparison:

(1) When the direct-drive turntable works, the torque motor transfers movement through the axis. The best axis optimization method is size optimization to ensure the direct-drive turntable's normal operation. The diameter was selected as the optimization parameter.
(2) The maximum radius of the workpiece is determined so we cannot change the turntable surface's diameter, but the thickness of the turntable surface can be optimized.
(3) Topology optimization results of the mounting sleeve are shown in light red and red. To avoid direct-drive turntable internal parts being exposed and the displacement of internal parts during sudden braking, the radius, rather than the installation sleeve's length, was considered optimized.
(4) The flanks of the swing frame have large mass redundancy, and the swing frame has little effect on the overall structure of the direct-drive turntable. Therefore, topology optimization was adopted for the swing frame.

Topology Optimization of Swing Frame

According to the topology optimization results, the swing frame was redesigned, and two optimization schemes were obtained, as shown in Figure 21.

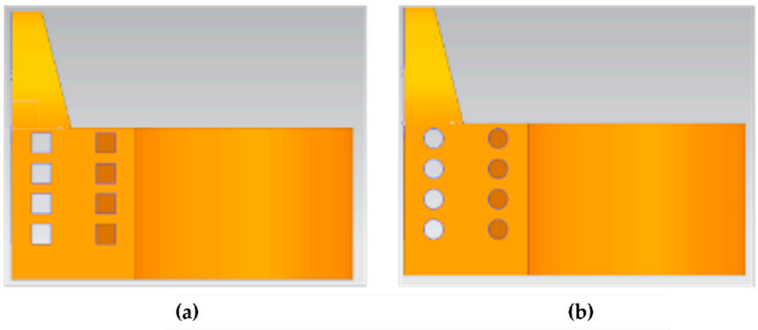

Figure 21. Topological structure of swing frame: (**a**) opening square hole; (**b**) opening round hole.

The simulation of two swing frames with different openings was carried out. Under the milling working condition, the static analysis of the direct-drive turntable with two different swing frames was carried out, and the relevant settings refer to the static characteristic analysis. Their maximum deformation is shown in Figure 22:

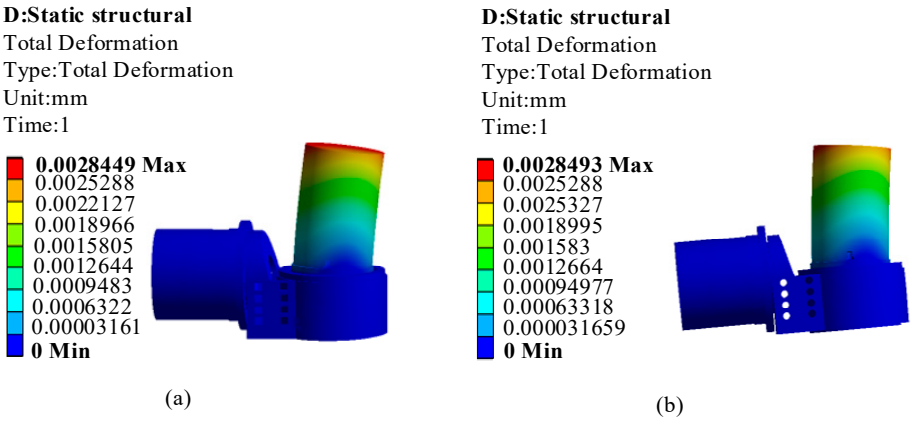

Figure 22. Deformation nephogram of direct-drive turntable with different swing frames in milling working condition: (**a**) opening square hole; (**b**) opening round hole.

It can be seen from Figure 22 that the maximum deformation of the direct-drive turntable with different swing frames is similar and has a certain decrease compared with the original structure. The optimized model has better static characteristics. The mass distributions of the left and right wings of the swing frame have little effect on the deformation of the direct-drive turntable. Therefore, a structure with greater mass removal was adopted, as shown in Figure 23:

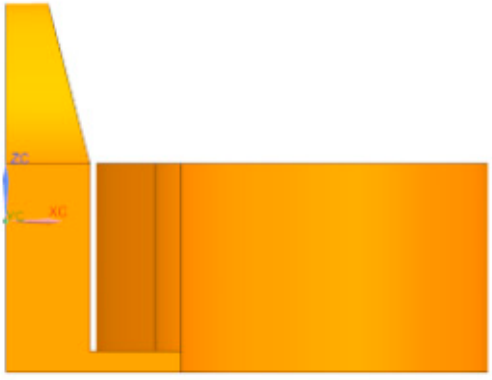

Figure 23. Improved swing frame.

Under the milling condition, the static and dynamic characteristic data of the direct-drive turntable with an optimized swing frame were obtained after static and dynamic analysis.

By comparing the two sets of data in Table 10, we can see that the mass of the optimized model is greatly reduced, reaching 13.5%. The maximum deformation and the first natural frequency also have a certain degree of optimization to achieve the purpose of optimization.

Table 10. Comparison of parameters before and after optimization of direct-drive turntable.

	Total Mass (kg)	Maximum Deformation (μm)	First Natural Frequency (Hz)
Before optimization	127.6	2.9772	594.33
Optimized	110.3	2.8232	614.25

3.4. Multi-Objective Optimization Results and Analysis

3.4.1. Sensitivity Analysis Results and Discussion

The sensitivity of seven optimization parameters to the turntable's natural frequency, the maximum deformation, and the total mass were analyzed. The results are as follows:

It can be seen from Figures 24–26 that parameters n_2, n_4, n_5, and n_7 are sensitive to the first-order natural frequency and are negatively correlated with the first-order natural frequency. Parameters n_2, n_4, n_5, and n_7 are sensitive to the maximum deformation and positively correlated with the maximum. Parameters n_1, n_3, and n_7 are sensitive to total mass, where n_1 and n_7 are negatively correlated with total mass and n_3 is positively correlated with total mass. Since parameter n_6 has a small contribution to the optimization, the other parameters are sensitive to the dynamic and static characteristics of the direct-drive turntable. Therefore, only parameters n_1–n_5 and n_7 were retained for size optimization.

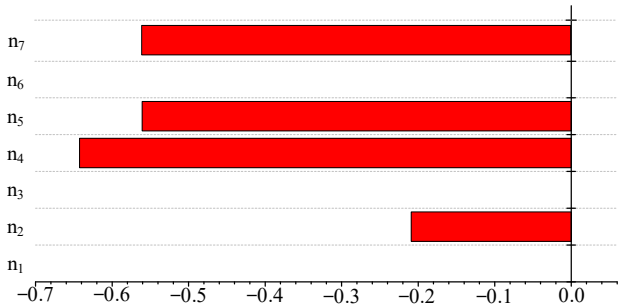

Figure 24. Correlation of 7 optimization parameters to natural frequency sensitivity.

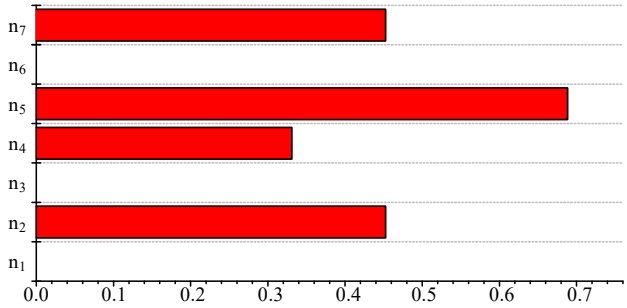

Figure 25. Correlation of 7 optimization parameters to maximum deformation sensitivity.

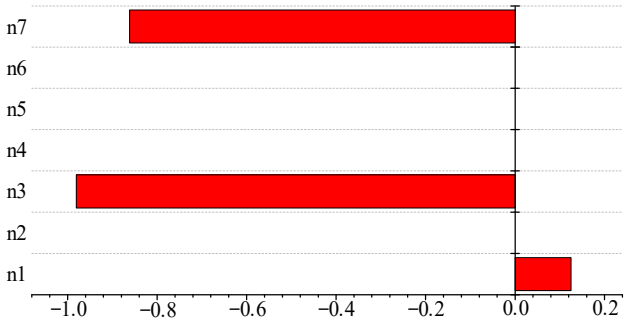

Figure 26. Correlation of 7 optimization parameters to total mass sensitivity.

3.4.2. Response Surface Fitting Results and Discussion

The response surface curves are shown in Figures 27–29:

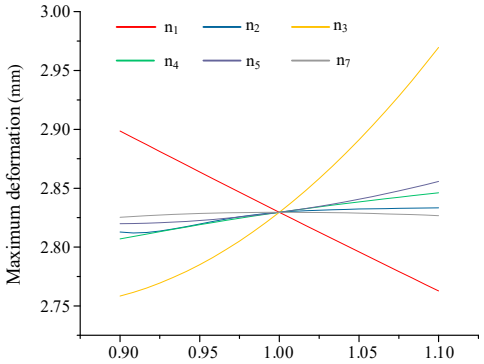

Figure 27. Deformation response curve.

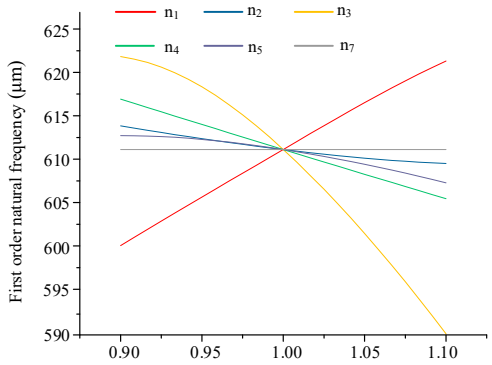

Figure 28. Frequency response curve.

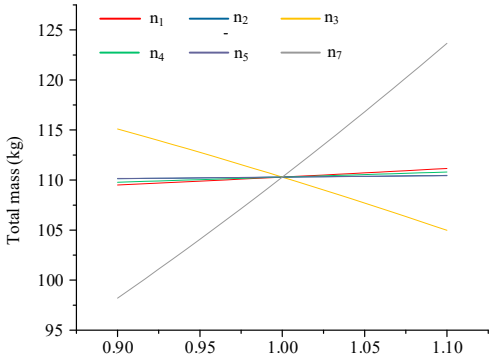

Figure 29. Mass response curve.

It can be seen from Figures 27–29 that the optimization parameters are related to the first-order natural frequency, maximum deformation, and mass, but the correlation is irregularly distributed. Increasing or decreasing a certain parameter cannot improve the dynamic and static characteristics or the mass of the direct-drive turntable. Since it is difficult for all the optimization parameters to achieve the optimal solution simultaneously, it is necessary to carry out further multi-objective optimization to obtain the optimal value.

The main index to evaluate the response surface is the decision coefficient R^2, with the best value being $R^2 = 1$. The response surface determination coefficients of the first-order natural frequency, minimum deformation, and total mass of the direct-drive turntable are 0.99873, 0.9887, and 1. The optimum root means the square error is 0, and the root means the square errors of response surface for the first natural frequency, minimum deformation, and total mass are 0.39775, 2.3254×10^{-6}, and 1.8594×10^{-13}, respectively. The response surface model has a good fitting degree in terms of the above parameters.

The closer the normalized curve of the test points and the verification points are to the X- and Y-angle bisector, the better the prediction result is. The prediction error is greater if it is far away from the X- and Y-angle bisector. The normalized curve of this test is shown in Figure 30.

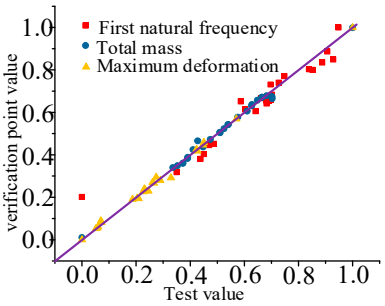

Figure 30. Normalized curve.

By observing Figure 30, we can see that a few points are not on the X- and Y-angle bisector. The other points are almost on the X- and Y-angle bisector, and the prediction accuracy is higher.

3.4.3. Multi-Objective Optimization Results and Discussion

The traditional multi-objective optimization method is to transform multi-objective optimization into single-objective optimization. Therefore, the traditional method has low computational efficiency, making it difficult to obtain a global optimization solution. So, a multi-objective genetic algorithm is proposed to solve practical problems. In multi-objective optimization, it is not easy to achieve the optimal solution among the objectives simultaneously, so multi-objective optimization often generates a series of effective solutions, also known as Pareto solutions. These solutions all meet the requirements, so we cannot compare them. In the multi-objective optimization problem, it is necessary to find as many Pareto solutions as possible that are unbiased and conform to the requirements. Then, according to the design requirements and practical engineering experience, the most satisfactory optimization results are objectively selected. NSGA-II is considered one of the most effective multi-objective genetic algorithms [26], and can reduce the computation scale and preserve the influential elite and population diversity.

Since the optimization objectives of the direct-drive turntable are the total mass, the first-order natural frequency, and the maximum deformation, the multi-objective genetic algorithm is used to solve the mathematical model of multi-objective optimization. The initial population is 100, the number of samples for one iteration is 100, the maximum allowable Pareto percentage is 50, and the maximum number of iterations is 20. Other options adopt the system default, and 100 Pareto solutions are generated. The Pareto solutions between two of the three objective functions are:

We selected three groups of optimal parameters and optimization objectives from many initial populations through the multi-objective genetic algorithm. The values are shown in Tables 11 and 12 and marked by green lines in Figure 31.

Table 11. Size parameters after and before optimization.

	Original Data (mm)	Optimization Data 1 (mm)	Optimization Data 2 (mm)	Optimization Data 3 (mm)
n_1	82.140	88.633	89.409	89.274
n_2	13.160	11.887	11.970	12.074
n_3	205.780	185.86	191.860	198.310
n_4	22.810	20.561	20.553	20.553
n_5	10.530	9.5326	9.517	9.572
n_7	235.000	212.13	213.560	212.140

Table 12. Original data and optimization values of optimization objectives.

	Mass (kg)	First Natural Frequency (Hz)	Deformation (μm)
Optimal value 1	103.050	641.970	2.6620
Optimal value 2	102.610	641.670	2.6660
Optimal value 3	100.340	637.820	2.6888
Original data	110.300	614.250	2.8232

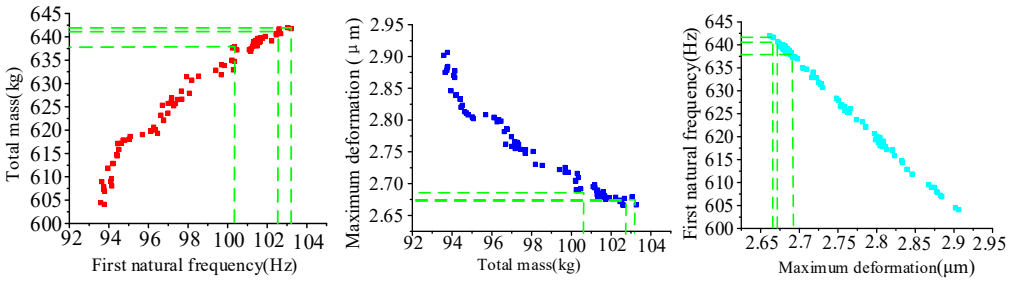

Figure 31. NSGA-II Pareto solution.

To prevent a large error between the selected optimized and real values, we used the above three sets of optimized parameter dimensions to re-model them in the SolidWorks software and perform the relevant finite element analysis. We compared the total mass, maximum deformation, and first natural frequency of the optimized direct-drive turntable with the fitting value. The relationship between the predicting value and the simulation value of the direct-drive turntable is shown in Figure 32:

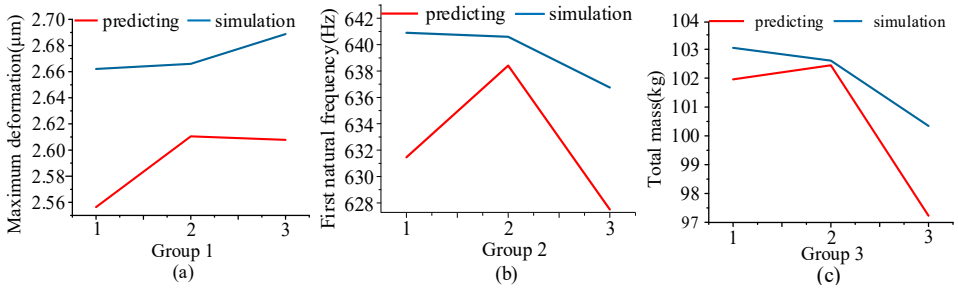

Figure 32. Prediction and simulation values: (**a**) deformation; (**b**) first natural frequency; (**c**) total mass.

Compared with the prediction and simulation values of the maximum deformation, the absolute errors of the predicting values of the first, second, and third groups

are 0.1057 μm, 0.055 μm, and 0.081 μm, and the prediction deviations are about 3.97%, 2.08%, and 3.01%, respectively. Compared with the predicting values and the simulation values of the first natural frequency, the absolute errors of the predicting values of the first, second, and third groups are 9.43 Hz, 2.18 Hz, and 9.25 Hz, and the prediction deviations are about 1.47%, 0.34%, and 1.45%, respectively. Compared with the predicting values and the simulation values of the total mass, the absolute errors of the predicting values of the first, second, and third groups are 1.086 kg, 0.1641 kg, and 3.11 kg, and the prediction deviations are about 1.05%, 0.16%, and 3.1%, respectively. It can be seen that there is a difference between the predicting value and the simulation value.

The optimization objectives were to reduce the mass and deformation of the turntable and improve the first natural frequency. Under three sets of optimization values, the maximum deformation, the first-order natural frequency, and the total mass of the direct-drive turntable are optimized to a certain extent. Among the three optimization values, optimization value 1 has the greatest degree of optimization on the deformation of the direct-drive turntable. Optimization value 3 has the greatest degree of optimization on the total mass of the direct-drive turntable. The optimization degree of optimization value 3 on all the objectives is between optimization values 1 and 2.

From the actual situation, the maximum deformation of the direct-drive turntable is far less than 10μm, and the processing speed corresponding to frequency cannot reach the first natural frequency. Therefore, optimization value 3 is the optimal solution. Compared with before topology optimization, the mass of the direct-drive turntable is reduced by 9.02%, the first natural frequency is increased by 3.83%, and the deformation is decreased by 4.76%. Compared with the original model, the total mass of the direct-drive turntable decreases significantly, reaching 21.394%.

To verify the effect of the optimization results on the machining conditions of the direct-drive turntable, we needed to extract and round the optimization data. So, n_1 = 89 mm, n_2 = 12 mm, n_3 = 198 mm, n_4 = 20.5 mm, n_5 = 9.6 mm, and n_7 = 212 mm. These parameters were brought into SolidWorks 2020 to remodel the direct-drive turntable. According to the previous chapter's static and dynamic analysis methods, the direct-drive turntable's dynamic and static characteristics under turning conditions were analyzed. The results of the maximum deformation and the first natural frequency were obtained; the maximum deformation is 4.0257×10^{-3} mm and the first natural frequency is 680.08 Hz. Comparing the maximum deformation and the first natural frequency before and after optimization in the turning condition, we can see that the maximum deformation of the direct-drive turntable decreased by 11.0%, and the first natural frequency increased by 14.3%. So, the dynamic and static characteristics of the structure increased to a certain extent.

4. Conclusions

Through static analysis, we found the maximum deformation position by adding cutting force to different processing positions of the direct-drive turntable. At the maximum deformation position, the stress was far less than the yield limit of the material, and the deformation degree was also within the allowable range of processing conditions. The finite element modal analysis of the direct-drive turntable shows that the lower natural frequency mainly affects the C-axis part of the direct-drive turntable. To further investigate the relationship between the machining frequency and the dynamic deformation of the direct-drive turntable, harmonic response analysis was performed on the direct-drive turntable. Safety analysis of the dynamic characteristics of the direct-drive turntable was carried out. The machining frequency is far from the natural frequency, so a direct-drive turntable can avoid that resonance during machining. Combined with the variable density method, the mathematical topology optimization model was established, and topology optimization of the single and composite conditions was carried out, respectively. The topology optimization results were analyzed, and the mass redundancy of the swing frame was reduced by topology optimization. Size optimization was used for the other

parts of the direct-drive turntable. The research results provide a theoretical basis for the multi-objective optimization of direct-drive turntables.

Multi-objective optimization based on a genetic algorithm was proposed to realize the lightweight design of a direct-drive turntable under the condition that the dynamic and static performance of the turntable meets the machining requirements. The optimized size parameters were selected according to the direct-drive turntable's structural characteristics and topology optimization results. The optimized size parameters were screened via sensitivity analysis. Through the central composite experimental design, 45 test points were obtained, and the 45 points were fitted to the response surface model using the BP neural network. Taking the total mass, the first natural frequency, and the maximum deformation of the direct-drive turntable as the optimization objectives, NSGA-II was used for multi-objective optimization of the direct-drive turntable, and we obtained the optimal solution. The results show that the maximum deformation and the first-order natural frequency of the direct-drive turntable is optimized to a certain extent, and the mass of the direct-drive turntable is significantly reduced by 21.394%. The dynamic and static characteristics of the direct-drive turntable are improved. The correctness of the optimization results is verified via modal experiments, indicating that the multi-objective optimization method has reasonable engineering practicability.

Author Contributions: Conceptualization, K.L., B.T. and J.Z.; methodology, K.L., J.W. (Junxiong Wang) and J.Z.; software, B.H. and J.W. (Jian Wang); validation, K.L., B.T. and J.Z.; formal analysis, B.H.; investigation, B.H.; resources, B.H.; data curation, B.H. and J.W. (Jian Wang); writing—original draft preparation, B.T. and J.W. (Jian Wang); writing—review and editing, B.T.; visualization, J.Z.; supervision, K.L.; project administration, B.H. and J.W. (Jian Wang); funding acquisition, B.H. All authors have read and agreed to the published version of the manuscript.

Funding: This research was funded by the Foundation of Artificial Intelligence Key Laboratory of Sichuan Province, grant number 2020RYY01, the Science & Technology Department of Sichuan Province, grant number 2021YFG0050, and the Graduate Innovation Fund of Sichuan University of Science & Engineering, grant number Y2022047.

Institutional Review Board Statement: Not applicable.

Informed Consent Statement: Not applicable.

Data Availability Statement: The data presented in this study are available on request from the corresponding author.

Acknowledgments: All the authors are greatly acknowledged for their financial support in making this research possible.

Conflicts of Interest: The authors declare no conflict of interest.

References

1. Pedrammehr, S.; Mahboubkhah, M.; Khani, N. A study on vibration of Stewart platform-based machine tool table. *Int. J. Adv. Manuf. Technol.* **2013**, *65*, 991–1007. [CrossRef]
2. Liu, Z.; Zhan, C.; Zhao, Y.; Li, X.; Xia, L.; Cai, L. Modeling and analysis of the dynamic behaviors of a quantitative type hydrostatic rotary table. *J. Mech. Eng.* **2015**, *51*, 75–83. [CrossRef]
3. Li, T.; Wu, C.; Shen, L.; Kong, X.; Ding, X. Improving machine tool dynamic performance using modal prediction and sensitivity analysis method. *J. Mech. Eng.* **2019**, *55*, 178–186. [CrossRef]
4. Chen, J.; Lin, S.; He, B. Geometric error measurement and identification for rotary table of multi-axis machine tool using double ballbar. *Int. J. Mach. Tools Manuf.* **2014**, *77*, 55. [CrossRef]
5. Ding, W.; Zhu, X.; Huang, X. Effect of servo and geometric errors of tilting-rotary tables on volumetric errors in five-axis machine tools. *Int. J. Mach. Tools Manuf.* **2016**, *104*, 44. [CrossRef]
6. Alessandro, V.; Gianni, C.; Antonio, S. Axis geometrical errors analysis through a performance test to evaluate kinematic error in a five axis tilting-rotary table machine tool. *Precis. Eng.* **2015**, *39*, 224–233. [CrossRef]
7. Kang, Y.; Chang, P.; Tsai, W.; Chen, C. Integrated "CAE" strategies for the design of machine tool spindle-bearing systems. *Finite Elem. Anal. Des.* **2001**, *37*, 485–511. [CrossRef]
8. Huo, D.; Cheng, K.; Wardle, F. A holistic integrated dynamic design and modelling approach applied to the development of ultraprecision micro-milling machines. *Int. J. Mach. Tools Manuf.* **2010**, *50*, 335–343. [CrossRef]

9. Altintas, Y.; Brecher, C.; Weck, M.; Witt, S. Virtual machine tool. *CIRP Ann.* **2005**, *54*, 651–674. [CrossRef]
10. Kim, D.; Jung, S.; Lee, J.; Chang, S. Parametric study on design of composite-foam-resin concrete sandwich structures for precision machine tool structures. *Compos. Struct.* **2006**, *75*, 408–414. [CrossRef]
11. Besharati, S.; Dabbagh, V.; Amini, H.; Sarhan, A.; Akbari, J. Multi-objective selection and structural optimization of the gantry in a gantry machine tool for improving static, dynamic, and weight and cost performance. *Concurr. Eng. Res. Appl.* **2016**, *24*, 83–93. [CrossRef]
12. Neugebauer, R.; Wabner, M.; Ihlenfeldt, S.; Friess, U.; Schneider, F. Bionics Based Energy Efficient Machine Tool Design. *Procedia CIRP* **2012**, *3*, 561–566. [CrossRef]
13. Shen, L.; Ding, X.; Li, T.; Kong, X.; Dong, X. Structural dynamic design optimization and experimental verification of a machine tool. *Int. J. Adv. Manuf. Technol.* **2019**, *104*, 3773–3786. [CrossRef]
14. Liu, S.; Lin, M. Bionic optimization design for a CNC turntable based on thermal-mechanical coupling effect. *J. Braz. Soc. Mech. Sci.* **2020**, *42*, 253. [CrossRef]
15. Yi, Q.; Li, C.; Ji, Q.; Zhu, D.; Jin, Y. Design optimization of lathe spindle system for optimum energy efficiency. *J. Clean. Prod.* **2020**, *250*, 119536. [CrossRef]
16. Meng, D.; Yang, S.; He, C.; Wang, H.; Lv, Z.; Guo, Y.; Nie, P. Multidisciplinary design optimization of engineering systems under uncertainty: A review. *Nt. J. Struct. Integr.* **2022**, *13*, 565–593. [CrossRef]
17. Liu, C.; Tan, F.; Wang, L.; Cai, Z. Research on optimization of column structure design for dynamic performance of machine tool. *J. Mech. Eng.* **2016**, *52*, 161–168. [CrossRef]
18. Jiang, H.; Guan, Y.; Qiu, Z.; Zhang, X.; Chen, Z.; Xu, G. Dynamic and static multi-objective optimization of a vertical machining center based on response surface method. *J. Mech. Eng.* **2011**, *47*, 125–133. [CrossRef]
19. Li, C.; Yang, J.; Feng, C. Optimization design for key structural components of CNC machine tools. *Mach. Des. Manuf.* **2020**, *7*, 41–43. [CrossRef]
20. Yu, H.; Wang, Y.; Chen, H.; Cun, H. Optimization for machine tool column combinong response surface model with multi-objective genetic algorithm. *J. Xi'an Jiaotong Univ.* **2012**, *46*, 80–85. Available online: http:/www.cnki.net/kcms/detail/61.1069.T.20120823.1805.005.html (accessed on 15 January 2022).
21. Liu, S.; Du, Y.; Lin, M. Study on lightweight structural optimization design system for gantry machine tool. *Concurr. Eng. Res. Appl.* **2019**, *27*, 170–185. [CrossRef]
22. Liu, C.; Lai, J.; Luo, Y. Design of a Measurement System for Six-Degree-of-Freedom Geometric Errors of a Linear Guide of a Machine Tool. *Sensors* **2019**, *19*, 5. [CrossRef]
23. Guo, L.; Zhnag, H.; Ye, P.; Duan, G. Light weight design of machine tool based on sensitivity analysis. *J. Tsinghua Univ.* **2011**, *51*, 846–850. [CrossRef]
24. Eddie, S. Empirical Model-Building and Response Surfaces. *J. R. Stat. Soc. Ser. D* **1988**, *37*, 82. [CrossRef]
25. Anijdan, S.; Madaah-Hosseini, H.; Bahrami, A. Flow stress optimization for 304 stainless steel under cold and warm compression by artificial neural network and genetic algorithm. *Mater. Des.* **2007**, *28*, 609–615. [CrossRef]
26. Deb, K.; Pratap, A.; Agarwal, S.; Meyarivan, T. A fast and elitist multiobjective genetic algorithm: NSGA-II. *IEEE T. Evolut. Comput.* **2002**, *6*, 182–197. [CrossRef]
27. Fu, Y.; Diwekar, U. An efficient sampling approach to multiobjective optimization. *Ann. Oper. Res.* **2004**, *132*, 109–134. [CrossRef]
28. Diwekar, U.; Kalagnanam, J. Robust design using an efficient sampling technique. *Comput. Chem. Eng.* **1996**, *20* (Suppl. S1), S389–S394. [CrossRef]
29. Paskov, S.H. Average case complexity of multivariate integration for smooth functions. *J. Complex.* **1993**, *9*, 291–312. [CrossRef]